HHS Public Access

Author manuscript

Atherosclerosis. Author manuscript; available in PMC 2017 September 01.

Published in final edited form as:

Atherosclerosis. 2016 September ; 252: 136–146. doi:10.1016/j.atherosclerosis.2016.07.930.

Endothelial glycocalyx, apoptosis and inflammation in an atherosclerotic mouse model

Limary M. Cancel[#a], **Eno E. Ebong**[#a,b,¥], **Solomon Mensah**[a], **Carly Hirshberg**[c], and **John M. Tarbell**[a,*]

[a]Department of Biomedical Engineering, The City College of New York, New York, NY

[b]Department of Neuroscience, Albert Einstein College of Medicine, Bronx, NY

[c]Graduate Division Summer Undergraduate Research Program, Albert Einstein College of Medicine, Bronx, NY

[#] These authors contributed equally to this work.

Abstract

Background and aims—Previous experiments suggest that both increased endothelial cell apoptosis and endothelial surface glycocalyx shedding could play a role in the endothelial dysfunction and inflammation of athero-prone regions of the vasculature. We sought to elucidate the possibly synergistic mechanisms by which endothelial cell apoptosis and glycocalyx shedding promote atherogenesis.

Methods—4- to 6-week old male C57Bl/6 apolipoprotein E knockout ($ApoE^{-/-}$) mice were fed a Western diet for 10 weeks and developed plaques in their brachiocephalic arteries.

Results—Glycocalyx coverage and thickness were significantly reduced over the plaque region compared to the non-plaque region (coverage plaque: 71±23%, non-plaque: 97±3%, p= 0.02; thickness plaque: 0.85±0.15 μm, non-plaque: 1.2±0.21 μm, p= 0.006). Values in the non-plaque region were not different from those found in wild type mice fed a normal diet (coverage WT: 92±3%, p= 0.7 *vs*. non-plaque $ApoE^{-/-}$, thickness WT: 1.1±0.06 μm, p= 0.2 *vs*. non-plaque $ApoE^{-/-}$). Endothelial cell apoptosis was significantly increased in $ApoE^{-/-}$ mice compared to wild type mice ($ApoE^{-/-}$:64.3±33.0, WT: 1.1±0.5 TUNEL-pos/cm, p= 2×10^{-7}). The number of apoptotic endothelial cells per unit length was 2 times higher in the plaque region than in the non-plaque region of the same vessel (p= 3×10^{-5}). Increased expression of matrix metalloproteinase 9 co-localized with glycocalyx shedding and plaque buildup.

[*]Corresponding author: Steinman Hall, Room 404C, 160 Convent Ave, New York, NY 10031. Tel: 212-650-6841. tarbell@ccny.cuny.edu (J. M. Tarbell). **Address to use during production process:** Limary M. Cancel, Steinman Hall, Room T444, 160 Convent Ave, New York, NY 10031, limarycancel@yahoo.com, Phone: 212-650-8192.

[¥]Current affiliation: Department of Chemical Engineering, Northeastern University, 360 Huntington Ave, Boston, MA 02115.

Conflict of interest

The authors declared they do not have anything to disclose regarding conflict of interest with respect to this manuscript.
Solomon Mensah has nothing to disclose.
Carly Hirshberg has nothing to disclose.

Conclusions—Our results suggest that, in concert with endothelial apoptosis that increases lipid permeability, glycocalyx shedding initiated by inflammation facilitates monocyte adhesion and macrophage infiltration that promote lipid retention and the development of atherosclerotic plaques.

Keywords

atherosclerosis; glycocalyx; endothelial cell apoptosis; inflammation

Introduction

The accumulation of lipoproteins in the arterial wall is a hallmark of atherosclerosis [1]. Due to the clinical importance of atherosclerosis, the biomechanical, cellular, and molecular mechanisms underlying atherogenesis have been the focus of intense research. Atherosclerotic plaques build up at predictable arterial sites—vessel branches and curvatures—where blood flow is disrupted and recirculating flows exist, creating a biomechanical environment that extends lipid residence time, weakens the vascular wall against lipid infiltration, promotes inflammation, and sustains atherosclerotic plaque growth [2]. The flux of low density lipoprotein (LDL) into the arterial wall depends on both the plasma concentration and the vessel wall permeability [3]. A correlation between enhanced permeability to macromolecules and the localization of atherosclerotic plaques is well established. In experimental animals, the focal sites of predilection for either spontaneous or dietary-induced atherosclerosis display increased permeability to plasma proteins, most notably albumin, horseradish peroxidase and LDL [4, 5]. We [6, 7] and others [8, 9] have previously shown that the permeability of endothelial cell (EC) monolayers is highly correlated with their rate of apoptosis.

The endothelial glycocalyx (GCX) is made up largely of cell-linked glycosaminoglycans (GAGs) including heparan sulfate (HS), hyaluronic acid (HA), and chondroitin sulfate (CS) [10]. The association of altered GCX characteristics with atherosclerosis-prone locations in arteries was recognized in the early 1980s. Lewis *et al.* [11] observed the coronary arteries of White Carneau pigeons and noted that the GCX, as assessed by ruthenium red staining, was thinnest in areas with high disease predilection, and that upon cholesterol challenge, the GCX thickness was reduced in all arterial zones. More recently, van den Berg *et al.* [12] observed enhanced intimal accumulation of LDL in the internal carotid branch of mice where the HS and HA components of the GCX were thin, in comparison to the adjacent regions of the common carotid where LDL accumulation was reduced and HS and HA were thick.

Previous studies have shown that the local hemodynamics play a role in EC apoptosis, GCX shedding and inflammation. High levels of steady shear have been shown to reduce the rate of EC apoptosis [13, 14], while irregular flow conditions increase EC apoptosis [15]. Similarly, atheroprotective flow conditions increase the expression [16] and synthesis rate [17, 18] of GCX components compared to atheroprone flow. In addition, several studies have shown that disturbed flow leads to a pro-inflammatory EC gene expression [19, 20].

No study, however, has compared the association of GCX degradation, EC apoptosis and inflammation in atherosclerotic plaque formation. Thus a major objective of the present work is to understand the possibly synergistic mechanisms by which EC apoptosis, GCX shedding and inflammation promote atherogenesis. To address this objective, we studied high fat fed apolipolipoprotein E knockout ($ApoE^{-/-}$) mice, a well-established animal model of atherosclerosis. We quantified the number of apoptotic ECs and measured the thickness and continuity of a major EC surface GAG, hyaluronic acid, in plaque and non-plaque regions of the brachiocephalic artery (BCA), using the descending aorta (DA) as a control region that did not develop plaques. In addition, we immunostained for matrix metalloproteinase 9 (MMP-9) and CD68 as markers of inflammation.

Materials and methods

Animals studies, euthanasia, and fixation

All animal protocols were approved by the Institutional Animal Care and Use Committee (IACUC) of The City College of New York. Six male C57Bl/6 background $ApoE^{-/-}$ mice were obtained from Jackson Laboratories (Bar Harbor, Maine) at 6 weeks of age. The animals were fed a high fat diet (Dyets, Inc., Bethlehem, Pa), which was high in saturated fats and cholesterol, to induce atherosclerotic plaque formation in their proximal arteries. After 10 weeks on the high fat diet, the $ApoE^{-/-}$ mice were placed on a 5-hour fast. Following the fast, mice were anesthetized with 2% chloralose and 10% urethane in PBS at the initial dosage 7 μl/g and an additional 30 μl/dose when needed. A mid-line surgical incision was then made from the abdominal wall to thoracic wall of each mouse. The heart was exposed after cutting the diaphragm. A blood sample was obtained from the right atrium for future lipid and lipoprotein analysis. The inferior vena cava and right atrium were severed to drain the blood and 20 to 30 mL of PBS containing 1% BSA were pressure perfused from the left ventricle through the circulation system. The vessels were then pressure perfused with 20 to 30 mL of 2% paraformaldehyde in PBS. For reference, strain-, gender-, and age-matched wildtype (WT) C57Bl/6 mice fed a normal chow diet were also studied.

Vessel dissection, cryopreservation, and cryostat sectioning

After the blood was completely washed away and the mice were thoroughly fixed, their aortas were excised from the aortic root to the thoracic aorta. We also excised the brachiocephalic branch where disease commonly localizes and plaque rupture ultimately occurs [21, 22]. Excised vessels were frozen in a block of optimal cutting temperature (OCT) compound, stored at −80°C, and later sectioned (6μm thick sections) to expose the vessel wall cross-section using a cryostat set at −20°C. Six serial sections (36 μm apart) were placed on positively charged glass slides (Color Frost Plus, Fisher Scientific, Pittsburgh, PA). Sections mounted on glass slides were dried overnight before further processing or before storage with desiccate at −80°C for future use.

Staining

Apoptotic cells were identified by the terminal deoxynucleotidyl transferase dUTP nick end labeling (TUNEL) technique using the in situ cell dectection kit from Roche (Indianapolis,

IN) according to the manufacturer's instructions. Briefly, frozen sections were fixed in 4% PFA for 20 min, washed in PBS for 30 min, blocked with 3% H_2O_2 in methanol for 10 min, permeabilized with 0.1% Triton X-100 in 0.1% sodium citrate for 2 min on ice, then incubated with the TUNEL reaction mixture for 1 hr at 37°C. After washing 3X in PBS, sections were counterstained with DAPI and mounted with Vectashield medium.

Platelet endothelial cell adhesion molecule (PECAM) was used to stain endothelial cells, and HA was stained as a marker of the GCX layer. In addition, vessels were stained for matrix MMP-9 and CD68 as markers of inflammation. For PECAM and HA staining, the sections were post fixed in 4% PFA for 10 minutes, washed 2X in PBS, and permeabilized with 0.3% Triton X-100 in PBS for 10 minutes. Antigen retrieval was performed by heating the sections in 10mM sodium citrate after which the slides were washed 2X with PBS and blocked with 10% goat serum for 1 hour. The slides were then incubated in 1:50 biotinylated hyaluronic acid binding protein (b-HABP, EMD Millipore, Billerica, MA) for 2 nights or in 1:100 rabbit polyclonal anti-PECAM for 1 night in a humidified chamber at 4°C. Following washing 5X in PBS, b-HABP was detected by incubation with 1:500 HRP-conjugated streptavidin and anti-PECAM was detected by incubation with 1:500 HRP-conjugated anti-rabbit secondary antibody, both from Jackson ImmunoResearch (West Grove, PA). The signal was amplified using the TSA Plus Cyanine 3 System (Perkin Elmer, Waltham, MA). Sections were counterstained with DAPI and mounted with Vectashield (Vector Labs, Burlingame, CA). For MMP-9 staining, the sections were post fixed in 4% PFA for 10 minutes and washed 2X in Tris-buffered Saline (TBS), followed by antigen retrieval by heating in Tris-EDTA (10mM Tris Base, 1mM EDTA, 0.05% Tween 20, ph 9.0). The slides were then washed in TBS-0.025% Triton X-100, blocked with 10% goat serum and 1% BSA for 2hrs, and incubated with primary rabbit anti-MMP-9 (1:1000, Abcam,) overnight at 4°C. Anti-MMP-9 was detected by incubation with 1:500 HRP-conjugated anti-rabbit secondary antibody, and signal amplification was performed as above. For CD68 staining, the sections were post fixed in ice cold acetone for 10 minutes and washed in PBS containing 0.1% Tween 2X, followed by blocking in 4% rabbit serum for 10 minutes. The sections were then incubated with primary rat anti-mouse CD68 (1:250, AbD Serotec, Raleigh, NC) for 1hr at RT. Anti-CD68 was detected by incubation with biotinylated rabbit anti-rat secondary antibody (1:200, Vector Labs) for 10 minutes, followed by incubation with HRP-conjugated streptavidin and signal amplification as described above.

Lipids were stained after sections were post-fixed in 2% PFA for 10 minutes. Following a 30-second pre-incubation of the sections in 60% isopropanol, the sections were incubated for 25 minutes in 0.24% (w/v) Oil Red O dissolved in 60% isopropanol. Sections were counterstained using Mayer's hemotoxylin and mounted with Vectashield medium.

Imaging and analysis

TUNEL positive cells were viewed and counted using a Nikon Eclipse TE2000-E or a Nikon TiE inverted microscope at 20x and 40x magnification. Images were taken with a CCD color camera on the Nikon TiE microscope at 20x magnification. The luminal perimeter of each vessel section was measured from the acquired images using NIH Image J software.

Apoptosis was expressed as the number of TUNEL positive cells per unit length (in cm) overlying the plaque or non-plaque regions of each vessel section.

HA, MMP-9, and CD68 staining was visualized using a Zeiss LSM 510 Confocal Laser Scanning system at 10X and 63X/oil magnification. Glycocalyx (HA) thickness and coverage, and MMP-9 intensity were analyzed using NIH ImageJ software. HA continuity was measured using a grid to standardize measurements. A ratio of the number of grid-cells containing continuous HA staining to the total number of grid-cells covering the inner vessel wall was computed to find a percent coverage per vessel. Gycocalyx thickness was determined after calibration with a stage micrometer or calibration bar (for each objective lens). One transverse line was drawn on the HA layer and measured in each grid-cell, giving approximately 10 measurements per image or section and 60 measurements from each of three glass slides for the vessel of interest. MMP-9 intensity was quantified by selecting a region of interest (ROI) containing only the luminal layer of endothelial cells. The MMP-9 intensity was expressed as the fraction of the ROI area having a value above the background intensity threshold, which was defined by the method described in [23].

Lipid labeling was examined using a Zeiss AxioImager, 5X and 10X objectives, and an Olympus DP72 digital camera to record images in color. Atherosclerotic plaque size, based on Oil red O staining, was quantified using NIH Image J software.

Lipid and lipoprotein analyses

Blood samples were obtained from the right atrium. Plasma cholesterol levels were determined using colorimetric enzymatic assays from Wako Diagnostics (Richmond, VA). Total cholesterol was measured with the Total Cholesterol-E assay; HDL cholesterol was measured with the HDL Cholesterol-E assay; LDL cholesterol was measured with the L-type LDL-C cholesterol assay.

Statistical analysis

Student’s t-test was used to compare differences between two groups. When applicable, because of non-normality of the data, non-parametric tests were used. For comparison of MMP-9 intensity data, 1-way ANOVA with Tukey’s method to correct for multiple comparisons was used. GraphPad Prism was used to perform statistical analysis and to generate data plots.

Results

General pathological findings

Mean serum total cholesterol concentrations were significantly higher in the *ApoE*$^{-/-}$ high fat fed mice than in the WT normal diet fed mice (Table 1). Total cholesterol concentration was 65.1±1.8 mg/dL in WT mice and increased significantly by 12-fold to 811.6±53.6 in *ApoE*$^{-/-}$ mice. HDL cholesterol decreased significantly from 31.5±4.6 mg/dL in WT to 6.5±0.7 mg/dL in *ApoE*$^{-/-}$. LDL cholesterol significantly increased from 25.1±2.5 mg/dL in WT to 412.6±14.6 mg/dL in *ApoE*$^{-/-}$. The amount of cholesterol contained in other lipid fractions such as VLDL, triglycerides and chylomicrons was estimated by subtracting HDL

and LDL cholesterol from the total cholesterol. The concentration of cholesterol in these fractions increased from 8.4±7.8 mg/dL in WT to 392.6±40.9 mg/dL in *ApoE*$^{-/-}$.

Despite the systemically elevated levels of plasma cholesterol in the high fat fed mice, only the predictable vessel wall regions exhibited lipid retention and atherosclerotic plaque growth. After 10 weeks on the high fat diet, the *ApoE*$^{-/-}$ mice exhibited raised plaques that were visible as white streaks under the dissection microscope (Figure 1C). Plaques were visible in the expected areas: the lower curvature of the aortic arch and the outer wall of the bifurcation in the BCA. Wild type mice fed a normal chow diet did not show any lesions (Figure 1B). In the present work, we studied lesions in the BCA and used sections of the descending thoracic aorta that were free of intercostals arteries as a non-diseased control area (Figure 1A).

Cryosections of the BCA were stained with Oil Red O to visualize the lipid filled plaques (Figure 1D). The average area of the plaques in *ApoE*$^{-/-}$ mice was found to be 82.2±18.6 × 10^3 μm^2, and occupying an average of 33% of the vessel luminal area, similar to previous studies [24]. PECAM immunostaining was performed to confirm the presence of an intact endothelial layer in both the plaque and non-plaque regions of the vessel (Figure 1E).

Apoptosis in the BCA

Figures 2A-2D show representative images of TUNEL staining in the BCA of *ApoE*$^{-/-}$ and WT mice. We counted apoptotic cells (bright green FITC label) and measured the perimeter of the lumen to determine the number of apoptotic ECs per unit length in each section. The number of TUNEL positive cells varied widely from animal to animal in the *ApoE*$^{-/-}$, ranging from 1.1 to 220.2 TUNEL-pos/cm. In the WT mice the number of TUNEL positive cells ranged from 0.23 to 2.60 The *ApoE*$^{-/-}$ mice BCA had an average of 64.3±33.0 TUNEL-pos/cm, significantly higher than the average in the WT BCA of 1.1±0.5 TUNEL-pos/cm (Figure 2E).

To determine whether apoptosis was occurring preferentially in the endothelial cells covering the plaque area, we measured the length of the plaque and non-plaque areas, and calculated the number of TUNEL-positive cells per unit length in each area. The non-plaque area had 47.95±8.34 TUNEL-pos/cm, while the number increased by 2-fold in the plaque area (94.38 + 15.8 TUNEL-pos/cm; Figure 2F). This increase in apoptosis was found to be highly significant by paired t-test (p<0.0001).

Apoptosis in the DA

Figures 3A-3D shows representative images of TUNEL staining in the DA of *ApoE*$^{-/-}$ and WT mice. In WT mice, endothelial apoptosis in the DA ranged from 0.33 to 9.6 with an average of 3.1±2.2 TUNEL-pos/cm. In the *ApoE*$^{-/-}$ mice, the DA had average endothelial apoptosis of 119.5±44.1, 38 times higher than in the WT (Figure 3E). As with the values in the BCA, the number of TUNEL positive cells varied widely from animal to animal ranging from 0.26 to 273.7 TUNEL-pos/cm.

HA staining in the BCA

Figure 4 shows representative images of HA staining in the BCA of *ApoE*$^{-/-}$ and WT mice. In the *ApoE*$^{-/-}$, the GCX can be seen overlying the non-plaque regions (Figure 4C) and it is degraded in the areas overlying the plaque (Figure 4B). GCX coverage was found to be 97±3% in the non-plaque regions of the *ApoE*$^{-/-}$ BCA, and was significantly decreased to 71±23% in the plaque regions (Figure 4H). Similarly, GCX thickness was 1.2±0.21 μm in the non-plaque regions and was significantly decreased to 0.85±0.15 μm in the plaque region (Figure 4I).

In the WT mice (Figures 4D and E) the GCX appears fully intact. GCX coverage was 92±3% in the WT BCA, and the thickness was 1.1±0.06 μm. These values were not significantly different from the values on the non-plaque regions of the *ApoE*$^{-/-}$ mice (Figures 4F and G).

HA staining in the DA

Figure 5 shows representative images of HA staining in the DA of *ApoE*$^{-/-}$ and WT mice. GCX appears intact for both groups in the athero-protected DA (Figures 5A-D). GCX coverage was found to be 91±2% in the WT and 96±2% in the *ApoE*$^{-/-}$. GCX thickness was found to be 1.1±0.07 μm in the WT and 0.93±0.05 μm in the *ApoE*$^{-/-}$. Neither value was found to be significantly different between the two groups (Figures 5E and F).

Inflammatory marker staining

A typical ROI selection for MMP-9 intensity quantification is shown in Figure 6A for the plaque (top panels) and non-plaque (bottom panels) regions of the BCA. The ROI was selected in the merged image (left panels) to include the endothelial cell layer only, and quantified in the red channel (MMP-9; right panels). Figures 6B-6G show representative images of MMP-9 immunostaining in the BCA of *ApoE*$^{-/-}$ and WT mice. MMP-9 is present throughout the plaque in the *ApoE*$^{-/-}$ mouse (Figures 6B and C) while it is markedly decreased in the non-plaque area of the *ApoE*$^{-/-}$ mouse as well as in the WT mouse (Figures 6D-F). DA sections from WT and *ApoE*$^{-/-}$ mice were also immunostained for MMP-9 (images not shown). Figure 6G shows the results of the quantification of MMP-9 intensity in all the vessels studied. There was no significant difference in MMP-9 intensity between the BCA in WT mice, and the non-plaque areas of the *ApoE*$^{-/-}$ mice. In the plaque area of the *ApoE*$^{-/-}$ BCA, MMP-9 intensity was 2-fold higher than in both the WT BCA and non-plaque areas of the *ApoE*$^{-/-}$ BCA. MMP-9 intensity in the WT DA was found to be the lowest of all the vessels examined. Intensity in the WT DA was 8-fold lower when compared to the *ApoE*$^{-/-}$ DA, and 13-fold lower when compared to the WT BCA. Immunostaining of CD68 in DA and BCA sections from *ApoE*$^{-/-}$ mice (Supplemental Figure 1) shows a pattern similar to MMP-9, i.e., strong staining in the plaques and little or no staining in the non-plaque areas.

Discussion

In the present study, after 10 weeks on a high fat diet, all of the *ApoE*$^{-/-}$ mice exhibited prominent plaques in the BCA. Oil Red O staining indicated that there was substantial lipid

accumulation in the plaques, but no observable Oil Red O staining in the non-plaque regions of the BCA or the DA. These plaques appeared to be typical of early to mid-stage disease progression (Fig. 1).

Transport of macromolecules across the endothelium can occur through three potential pathways [5]: 1) transcytosis in vesicles, 2) paracellular transport through the normal breaks in the tight junction strand, and 3) through the leaky junction associated with cells undergoing apoptosis or mitosis. It is unlikely that a normal junction break would permit the passage of LDL (22 nm diameter), even without the GCX as a molecular filter, because the widest part of the junction is expected to be about 20 nm [25]. Weinbaum *et al.* [9] were first to propose the leaky junction as the primary transport pathway for LDL. *In vivo* studies by Chien and coworkers [8, 26] supported the importance of the leaky junction pathway in LDL and albumin transport in the rat aorta. *In vitro,* our lab showed that the leaky junction is the dominant transport pathway for LDL [7], and that there is a strong correlation between EC apoptosis and LDL permeability [6]. Despite all the evidence, few studies have examined EC-specific apoptosis in relation to early atherosclerotic plaque development in vivo. Here we demonstrated that the number of apoptotic ECs per unit length is significantly higher in the plaque region of the BCA of *ApoE*$^{-/-}$ mice than in the non-plaque region of the same vessel (Figure 3F), which would be expected to result in higher permeability of the plaque region to macromolecules. Overall EC apoptosis rates (as a percentage of total ECs) were 18.2±8.5% in the BCA and 39.8±14.3% in the DA. These values, while extremely high, are in agreement with those reported in recent studies that examined the atheroprone aortic root of *ApoE*$^{-/-}$ mice fed a western diet for 6-8 weeks [27] [28]. Those studies also found a 15-fold increase in cleaved caspase-3 expression compared to WT mice. While an increase in apoptosis in atheroprone areas is expected [15], the most surprising result is that we observed EC apoptosis to be elevated everywhere in the ApoE$^{-/-}$ mice, including the athero-protected DA. To our knowledge, the present study is the first to look at EC apoptosis in non-plaque regions of the *ApoE*$^{-/-}$ model. We hypothesize that the systemic increase in EC apoptosis is due to the highly atherogenic lipid profile developed in the *ApoE*$^{-/-}$ mice on a Western diet. LDL and VLDL cholesterol, which have been shown to induce EC apoptosis [29], increased by 16- and 46-fold, respectively, while HDL cholesterol, which has been shown to inhibit EC apoptosis [30], decreased by nearly 5-fold (Table 1). It is also possible that increased EC apoptosis is inherent to the *ApoE*$^{-/-}$ model and the condition is exacerbated by the lipid profile. Further studies of EC apoptosis in *ApoE*$^{-/-}$ mice fed a normal diet as well as measurement of EC apoptosis at several time points after the start of the Western diet are necessary to establish the causes of systemic elevated apoptosis in the *ApoE*$^{-/-}$ model.

We observed significantly lower coverage and thickness of the glycocalyx (HA layer) in the plaque region of the BCA compared to the non-plaque region of the BCA or the DA in the *ApoE*$^{-/-}$ mouse, where these values were not different from values in the WT mouse (Figs. 4 and 5). This is consistent with the earlier observations of van den Berg *et al.* [31] that the glycocalyx was reduced in the disease prone sinus region of the mouse internal carotid. We also found that MMP-9 was significantly elevated in the intimal layer overlying the plaque in the BCA and, to a lesser degree, in the DA of the *ApoE*$^{-/-}$ and the BCA of the WT mouse.

There are several possible interpretations of our observations and their relevance to the development of atherosclerosis. First, the reduced glycocalyx and elevated MMP-9 in the BCA may be considered as indicators of local inflammation induced by the fluid mechanical environment. This interpretation is consistent with findings reported by Gouverneur and coworkers [18], which demonstrated that GCX components regrow at a higher rate in arteries exposed to healthy levels of vessel wall shear stress, compared to low levels of wall shear stress. Recent in vitro studies showed similar phenomena. Koo *et al.* [16] observed that an atheroprotective shear stress waveform increased the expression of heparan sulfate on HUVECs via upregulation of its syndecan-1 proteoglycan, while an atheroprone waveform had the opposite effect. The same group showed faster regrowth of heparan sulfate after enzymatic degradation under laminar shear compared to static conditions [17]. Therefore, the growth and shedding of GCX components are actively regulated by ECs in response to the local hemodynamics.

Furthermore, ECs exposed to disturbed flow upregulate their expression of important chemokines and chemokine receptors and activate the NF-κB signaling pathway [32] which mediates the inflammatory response [33, 34]. Magid et al [35] showed a 3-fold increase in MMP-9 protein and mRNA expression in ECs exposed to oscillatory shear stress compared to unidirectional shear, suggesting MMP-9 expression by ECs is sensitive to flow and may contribute to the initiating events in lesion development. Cui *et al.* [36] and Mulivor and Lipowsky [37] found that MMPs degrade glycocalyx while Lipowsky and Lescanic [38] described degradation of the glycocalyx by reactive oxygen species (ROS). Recent studies from Jo's group [39] using an $ApoE^{-/-}$ mouse model with partial ligation of the left carotid artery to induce a reversing oscillatory flow field in the common carotid artery showed rapid development of atherosclerotic plaques due to a mechanism involving oscillatory shear-induced upregulation of microRNA 712 that suppresses tissue inhibitor of metalloproteinase 3, thus allowing increased MMP activity.

Second, a low level inflammation (MMP-9, Fig. 6) in all areas of $ApoE^{-/-}$ compared to WT mice may be considered an indicator of systemic inflammation induced by the elevated cholesterol. Higher serum levels of MMP-9 and lower levels of TIMP-1, an endogenous inhibitor of MMPs, were found in patients with familial hypercholesterolemia [40]. Um *et al.* [41] showed increased MMP-9 and MMP-1 mRNA expression in the aortas of rabbits fed a high cholesterol diet for 8 weeks. The GCX could also be affected by cholesterol levels indirectly by the activation of MMPs capable of cleaving GCX components [37, 42-45]. More directly the GCX is affected by the reduction in HDL levels (Table 1) because it can be in part regulated by cardioprotective [46, 47] sphingosine-1-phosphate (S1P). S1P is released from erythrocytes into plasma and then transported by albumin and HDL through plasma to ECs. On ECs S1P preserves the GCX by inducing synthesis and inhibiting shedding [45, 48, 49]. In our study, however, systemic inflammation alone (as in the DA) does not result in detectable degradation of the GCX or recruitment of monocytes/macrophages in $ApoE^{-/-}$ mice (Fig 5 and Supplemental Fig. 1).

Third, the diminished glycocalyx barrier can propagate further inflammation by providing circulating leukocytes and platelets with enhanced access to adhesion receptors on the endothelial surface thus recruiting them to the intima [50]. Reitsma *et al.* [51] found reduced

GCX thickness and increased platelet adhesion in the carotid bifurcation of *ApoE*$^{-/-}$ mice fed a normal diet. Nagy *et al.* [52] showed that inhibiting endothelial hyaluronan synthesis with 4-methylumbelliferone reduced the GCX and resulted in increased leukocyte adhesion, macrophage retention, and accelerated plaque development in *ApoE*$^{-/-}$ mice fed a Western diet for 25 weeks. Similarly, Voyvodic *et al.* [53] showed increased leukocyte recruitment and inflammatory response in a syndecan-1 knockout mouse. Axelsson *et al.* [54] used a tissue-specific knockout of Hs2st to modify the structure of heparan sulfate in the ECs of a mouse by eliminating 2-O-sulfate groups. The modification resulted in increased neutrophil recruitment in response to inflammatory stimuli. Inflammatory cells recruited to the intima would be expected to release mediators, including ROS and MMPs [55-57] which are known to degrade the GCX [38, 56]. Therefore, by a positive feedback mechanism the initial flow-induced GCX degradation can lead to recruitment of inflammatory cells that further degrade the GCX and propagate the inflammatory response.

Degradation of the EC GCX is observed in many vascular-related diseases including diabetes and renal dysfunction [58]. Hyperglycemia resulted in a decrease in heparan sulfate content along with an attenuation of eNOS activation, hydraulic conductivity response, and cell alignment in an *in vitro* model of diabetes [59]. Forbes *et al.* [60] used an *ApoE*$^{-/-}$ mouse western diet with streptozotocin-induced diabetes and showed a 10-fold increase in plaque area in the athero-protected thoracic aorta compared to non-diabetic controls. Similarly, atherosclerosis in diabetic human subjects is not confined to areas of low shear and disturbed flow but found to be more uniformly distributed [61]. Increased GCX shedding was also observed in patients with chronic kidney disease [62] and dialysis patients [63], conditions that are associated with increased cardiovascular morbidity. These observations underscore the importance of the GCX in maintaining EC barrier function, limiting access to leukocytes that propagate inflammation, and promoting EC mechanotransduction mechanisms that protect against disease.

We note two unexpected results from our study: 1) apoptosis is high in the *ApoE*$^{-/-}$ DA and 2) there is a low level of inflammation (increased MMP-9) in this same vessel that is nonetheless higher than in the WT DA. We hypothesized above that both of these results can be attributed to systemic elevation of atherogenic lipid fractions (LDL, VLDL, etc.). Elevated apoptosis suggests increased permeability of the endothelium to LDL. Indeed it has been shown that the aorta in the high-fat fed *ApoE*$^{-/-}$ mouse model does experience increased solute permeability [64], consistent with increased apoptosis. However, the DA, away from intercostal ostia, remains protected from atherosclerosis. Our observation that the glycocalyx is not diminished in the DA provides a clue to explain these unexpected results. It suggests that even in the *ApoE*$^{-/-}$ animal on a high fat diet, the DA is a region of low enhancement of inflammation whereas the plaque region of the BCA that has a diminished glycocalyx experiences highly elevated inflammation. It is the combined effect of local inflammation, induced by disturbed flow in the BCA, along with systemic inflammation, induced by elevated cholesterol levels, which together produce the environment for LDL retention and plaque formation. Within this environment of enhanced inflammation, the GCX is diminished enough for inflammatory cells to be recruited. In addition to degrading the GCX, inflammatory mediators (e.g. ROS and MMPs) are capable of degrading HS proteoglycans [57] and other GAGs and proteins [43] present in the extracellular matrix.

Such alterations of the extracellular matrix have been shown to increase retention of LDL in the subendothelial intima [65]. In addition, ROS and MMPs can modify LDL particles, increasing their affinity to matrix proteoglycans, and triggering their aggregation and fusion [66].

In contrast, the inflammatory phenotype induced by disturbed flow on the outer wall of the BCA is not present in the DA where inflammatory indicators (glycocalyx thinning and MMP-9 localization) are absent or present at low levels, but apoptosis is still high. We have previously shown that high apoptosis rates lead to an increase in water flux and LDL permeability of EC monolayers in vitro [6]. In the rabbit thoracic aorta, Tedqui and Lever [67] showed that, in vessels with a damaged endothelium, enhanced water flux led to lower albumin retention in the vessel wall. It is known that ECs not exposed to disturbed flow, such as the DA, upregulate genes that are anti-thrombotic, anti-inflammatory and anti-oxidant [68]. Thus, our results suggest that these athero-protected areas may still experience high permeability due to elevated apoptosis induced by systemic risk factors such as high cholesterol levels, but do not develop plaques because LDL is not retained in the subendothelial intima without local inflammation and is instead washed away by the increased water flux.

The main limitation of the present study is that it looks at a single time point. Further studies should consider analysis of earlier plaques to assess the time course of GCX thinning, apoptosis elevation and MMP-9 elevation. In addition, while the $ApoE^{-/-}$ model on a high fat diet provides accelerated development of plaques and has been extensively characterized, the cholesterol levels developed in this model are much higher than seen in humans. It may be useful to consider an alternative model such as the $LDLR^{-/-}$ mouse, which develops cholesterol levels closer to those observed in humans [21]. Lowering cholesterol levels and measuring GCX, EC apoptosis, and MMP-9 at several time points may help to further clarify the relative importance of systemic and local factors in atherogenesis.

In summary, our apoptosis, glycocalyx and MMP-9 data in the $ApoE^{-/-}$ mouse model suggest that systemic inflammation leading to elevated apoptosis and LDL permeability, in concert with flow-induced local inflammation leading to elevated MMP-9 localization to the intima and reduced glycocalyx thickness, facilitate monocyte/macrophage accumulation in the intima, and lead to increased LDL retention and ultimately plaque formation on the outer wall of the BCA.

Supplementary Material

Refer to Web version on PubMed Central for supplementary material.

Acknowledgments

Financial support

Research supported by NIH HL094889.

Drs. Tarbell, Cancel and Ebong report support from NIH grant HL094889 during the conduct of the study.

References

1. Santos-Gallego CG, Picatoste B, Badimon JJ. Pathophysiology of acute coronary syndrome. Curr Atheroscler Rep. 2014; 16(4):401. [PubMed: 24504549]
2. Chiu JJ, Chien S. Effects of disturbed flow on vascular endothelium: pathophysiological basis and clinical perspectives. Physiol Rev. 2011; 91(1):327–87. [PubMed: 21248169]
3. Michel CC, Curry FE. Microvascular permeability. Physiol Rev. 1999; 79(3):703–61. [PubMed: 10390517]
4. Ogunrinade O, Kameya GT, Truskey GA. Effect of fluid shear stress on the permeability of the arterial endothelium. Ann Biomed Eng. 2002; 30(4):430–46. [PubMed: 12085996]
5. Tarbell JM. Mass transport in arteries and the localization of atherosclerosis. Annu Rev Biomed Eng. 2003; 5:79–118. [PubMed: 12651738]
6. Cancel LM, Tarbell JM. The role of apoptosis in LDL transport through cultured endothelial cell monolayers. Atherosclerosis. 2010; 208(2):335–41. [PubMed: 19709659]
7. Cancel LM, Fitting A, Tarbell JM. In vitro study of LDL transport under pressurized (convective) conditions. Am J Physiol Heart Circ Physiol. 2007; 293(1):H126–32. [PubMed: 17322415]
8. Lin S-J, Jan K-m, Chien S. Role of Dying Endothelial Cells in Transendothelial Macromolecular Transport. Arteriosclerosis. 1990; 10:703–9. [PubMed: 1698353]
9. Weinbaum S, Tzeghai G, Ganatos P, Pfeffer R, Chien S. Effect of Cell Turnover and Leaky Junctions on Arterial Macromolecular Transport. American Journal of Physiology. 1985; 248:H945–H58. [PubMed: 4003572]
10. Tarbell JM, Pahakis MY. Mechanotransduction and the glycocalyx. J Intern Med. 2006; 259(4): 339–50. [PubMed: 16594902]
11. Lewis JC, Taylor RG, Jones ND, St Clair RW, Cornhill JF. Endothelial surface characteristics in pigeon coronary artery atherosclerosis. I. Cellular alterations during the initial stages of dietary cholesterol challenge. Lab Invest. 1982; 46(2):123–38. [PubMed: 7062718]
12. van den Berg BM, Spaan JA, Vink H. Impaired glycocalyx barrier properties contribute to enhanced intimal low-density lipoprotein accumulation at the carotid artery bifurcation in mice. Pflugers Arch. 2009; 457(6):1199–206. [PubMed: 18839207]
13. Cho A, Mitchell L, Koopmans D, Langille BL. Effects of changes in blood flow rate on cell death and cell proliferation in carotid arteries of immature rabbits. Circ Res. 1997; 81(3):328–37. [PubMed: 9285634]
14. Dimmeler S, Haendeler J, Rippmann V, Nehls M, Zeiher AM. Shear stress inhibits apoptosis of human endothelial cells. FEBS Lett. 1996; 399(1-2):71–4. [PubMed: 8980122]
15. Freyberg MA, Kaiser D, Graf R, Buttenbender J, Friedl P. Proatherogenic flow conditions initiate endothelial apoptosis via thrombospondin-1 and the integrin-associated protein. Biochem Biophys Res Commun. 2001; 286(1):141–9. [PubMed: 11485320]
16. Koo A, Dewey CF Jr. Garcia-Cardena G. Hemodynamic shear stress characteristic of atherosclerosis-resistant regions promotes glycocalyx formation in cultured endothelial cells. Am J Physiol Cell Physiol. 2013; 304(2):C137–46. [PubMed: 23114962]
17. Giantsos-Adams KM, Koo AJ, Song S, Sakai J, Sankaran J, Shin JH, et al. Heparan Sulfate Regrowth Profiles Under Laminar Shear Flow Following Enzymatic Degradation. Cell Mol Bioeng. 2013; 6(2):160–74. [PubMed: 23805169]
18. Gouverneur M, Berg B, Nieuwdorp M, Stroes E, Vink H. Vasculoprotective properties of the endothelial glycocalyx: effects of fluid shear stress. J Intern Med. 2006; 259(4):393–400. [PubMed: 16594907]
19. Davies PF, Civelek M, Fang Y, Fleming I. The atherosusceptible endothelium: endothelial phenotypes in complex haemodynamic shear stress regions in vivo. Cardiovasc Res. 2013; 99(2): 315–27. [PubMed: 23619421]
20. Gimbrone MA Jr. Topper JN, Nagel T, Anderson KR, Garcia-Cardena G. Endothelial dysfunction, hemodynamic forces, and atherogenesis. Ann N Y Acad Sci. 2000; 902:230–9. discussion 9-40. [PubMed: 10865843]

21. Santos-Gallego CG, Badimon JJ, Ibanez B. Modelos experimentales de aterosclerosis. Rev Esp Cardio Supl. 2013; 13(E):3–12.
22. Bond AR, Jackson CL. The fat-fed apolipoprotein E knockout mouse brachiocephalic artery in the study of atherosclerotic plaque rupture. J Biomed Biotechnol. 2011; 2011:379069. [PubMed: 21076539]
23. Zeng Y, Ebong EE, Fu BM, Tarbell JM. The structural stability of the endothelial glycocalyx after enzymatic removal of glycosaminoglycans. PLoS One. 2012; 7(8):e43168. [PubMed: 22905223]
24. Williams H, Johnson JL, Carson KG, Jackson CL. Characteristics of intact and ruptured atherosclerotic plaques in brachiocephalic arteries of apolipoprotein E knockout mice. Arterioscler Thromb Vasc Biol. 2002; 22(5):788–92. [PubMed: 12006391]
25. Fu BM, Weinbaum S, Tsay RY, Curry FE. A junction-orifice-fiber entrance layer model for capillary permeability: application to frog mesenteric capillaries. J Biomech Eng. 1994; 116(4): 502–13. [PubMed: 7869727]
26. Chien S, Lin SJ, Weinbaum S, Lee MM, Jan KM. The role of arterial endothelial cell mitosis in macromolecular permeability. Adv Exp Med Biol. 1988; 242:59–73. [PubMed: 3245515]
27. Sun GB, Qin M, Ye JX, Pan RL, Meng XB, Wang M, et al. Inhibitory effects of myricitrin on oxidative stress-induced endothelial damage and early atherosclerosis in ApoE−/−mice. Toxicol Appl Pharmacol. 2013; 271(1):114–26. [PubMed: 23639522]
28. Ma L, Guo X, Chen W. Inhibitory effects of oleoylethanolamide (OEA) on H(2)O(2)-induced human umbilical vein endothelial cell (HUVEC) injury and apolipoprotein E knockout (ApoE−/−) atherosclerotic mice. Int J Clin Exp Pathol. 2015; 8(6):6301–11. [PubMed: 26261506]
29. Galle J, Schneider R, Heinloth A, Wanner C, Galle PR, Conzelmann E, et al. Lp(a) and LDL induce apoptosis in human endothelial cells and in rabbit aorta: role of oxidative stress. Kidney Int. 1999; 55(4):1450–61. [PubMed: 10201010]
30. Nofer JR, Levkau B, Wolinska I, Junker R, Fobker M, von Eckardstein A, et al. Suppression of endothelial cell apoptosis by high density lipoproteins (HDL) and HDL-associated lysosphingolipids. J Biol Chem. 2001; 276(37):34480–5. [PubMed: 11432865]
31. van den Berg BM, Spaan JA, Rolf TM, Vink H. Atherogenic region and diet diminish glycocalyx dimension and increase intima-to-media ratios at murine carotid artery bifurcation. Am J Physiol Heart Circ Physiol. 2006; 290(2):H915–20. [PubMed: 16155109]
32. Dai G, Kaazempur-Mofrad MR, Natarajan S, Zhang Y, Vaughn S, Blackman BR, et al. Distinct endothelial phenotypes evoked by arterial waveforms derived from atherosclerosis-susceptible and -resistant regions of human vasculature. Proc Natl Acad Sci U S A. 2004; 101(41):14871–6. [PubMed: 15466704]
33. Kempe S, Kestler H, Lasar A, Wirth T. NF-kappaB controls the global pro-inflammatory response in endothelial cells: evidence for the regulation of a pro-atherogenic program. Nucleic Acids Res. 2005; 33(16):5308–19. [PubMed: 16177180]
34. Brasier AR. The nuclear factor-kappaB-interleukin-6 signalling pathway mediating vascular inflammation. Cardiovasc Res. 2010; 86(2):211–8. [PubMed: 20202975]
35. Magid R, Murphy TJ, Galis ZS. Expression of matrix metalloproteinase-9 in endothelial cells is differentially regulated by shear stress. Role of c-Myc. J Biol Chem. 2003; 278(35):32994–9. [PubMed: 12816956]
36. Cui N, Wang H, Long Y, Su L, Liu D. Dexamethasone Suppressed LPS-Induced Matrix Metalloproteinase and Its Effect on Endothelial Glycocalyx Shedding. Mediators Inflamm. 2015; 2015:912726. [PubMed: 26199464]
37. Mulivor AW, Lipowsky HH. Inhibition of glycan shedding and leukocyte-endothelial adhesion in postcapillary venules by suppression of matrixmetalloprotease activity with doxycycline. Microcirculation. 2009; 16(8):657–66. [PubMed: 19905966]
38. Lipowsky HH, Lescanic A. The effect of doxycycline on shedding of the glycocalyx due to reactive oxygen species. Microvasc Res. 2013; 90:80–5. [PubMed: 23899417]
39. Son DJ, Kumar S, Takabe W, Kim CW, Ni CW, Alberts-Grill N, et al. The atypical mechanosensitive microRNA-712 derived from pre-ribosomal RNA induces endothelial inflammation and atherosclerosis. Nat Commun. 2013; 4:3000. [PubMed: 24346612]

40. Nenseter MS, Narverud I, Graesdal A, Bogsrud MP, Halvorsen B, Ose L, et al. Elevated serum MMP-9/TIMP-1 ratio in patients with homozygous familial hypercholesterolemia: effects of LDL-apheresis. Cytokine. 2013; 61(1):194–8. [PubMed: 23131422]
41. Um MY, Hwang KH, Choi WH, Ahn J, Jung CH, Ha TY. Curcumin attenuates adhesion molecules and matrix metalloproteinase expression in hypercholesterolemic rabbits. Nutr Res. 2014; 34(10): 886–93. [PubMed: 25282128]
42. Endo K, Takino T, Miyamori H, Kinsen H, Yoshizaki T, Furukawa M, et al. Cleavage of syndecan-1 by membrane type matrix metalloproteinase-1 stimulates cell migration. J Biol Chem. 2003; 278(42):40764–70. [PubMed: 12904296]
43. Gronski TJ Jr. Martin RL, Kobayashi DK, Walsh BC, Holman MC, Huber M, et al. Hydrolysis of a broad spectrum of extracellular matrix proteins by human macrophage elastase. J Biol Chem. 1997; 272(18):12189–94. [PubMed: 9115292]
44. Yu WH, Woessner JF Jr. Heparan sulfate proteoglycans as extracellular docking molecules for matrilysin (matrix metalloproteinase 7). J Biol Chem. 2000; 275(6):4183–91. [PubMed: 10660581]
45. Zeng Y, Adamson RH, Curry FR, Tarbell JM. Sphingosine-1-phosphate protects endothelial glycocalyx by inhibiting syndecan-1 shedding. Am J Physiol Heart Circ Physiol. 2014; 306(3):H363–72. [PubMed: 24285115]
46. Badimon JJ, Santos-Gallego CG. HDL Dysfunction: Is the Answer in the Sphinx's Riddle? J Am Coll Cardiol. 2015; 66(13):1486–8. [PubMed: 26403345]
47. Santos-Gallego CG, Vahl TP, Goliasch G, Picatoste B, Arias T, Ishikawa K, et al. Sphingosine-1-Phosphate Receptor Agonist Fingolimod Increases Myocardial Salvage and Decreases Adverse Postinfarction Left Ventricular Remodeling in a Porcine Model of Ischemia/Reperfusion. Circulation. 2016; 133(10):954–66. [PubMed: 26826180]
48. Zeng Y, Liu XH, Tarbell J, Fu B. Sphingosine 1-phosphate induced synthesis of glycocalyx on endothelial cells. Exp Cell Res. 2015; 339(1):90–5. [PubMed: 26364737]
49. Zhang L, Zeng M, Fan J, Tarbell JM, Curry FR, Fu BM. Sphingosine-1-phosphate Maintains Normal Vascular Permeability by Preserving Endothelial Surface Glycocalyx in Intact Microvessels. Microcirculation. 2016; 23(4):301–10. [PubMed: 27015105]
50. Lipowsky HH. The endothelial glycocalyx as a barrier to leukocyte adhesion and its mediation by extracellular proteases. Ann Biomed Eng. 2012; 40(4):840–8. [PubMed: 21984514]
51. Reitsma S, Oude Egbrink MG, Heijnen VV, Megens RT, Engels W, Vink H, et al. Endothelial glycocalyx thickness and platelet-vessel wall interactions during atherogenesis. Thromb Haemost. 2011; 106(5):939–46. [PubMed: 21901228]
52. Nagy N, Freudenberger T, Melchior-Becker A, Rock K, Ter Braak M, Jastrow H, et al. Inhibition of hyaluronan synthesis accelerates murine atherosclerosis: novel insights into the role of hyaluronan synthesis. Circulation. 2010; 122(22):2313–22. [PubMed: 21098434]
53. Voyvodic PL, Min D, Liu R, Williams E, Chitalia V, Dunn AK, et al. Loss of syndecan-1 induces a pro-inflammatory phenotype in endothelial cells with a dysregulated response to atheroprotective flow. J Biol Chem. 2014; 289(14):9547–59. [PubMed: 24554698]
54. Axelsson J, Xu D, Kang BN, Nussbacher JK, Handel TM, Ley K, et al. Inactivation of heparan sulfate 2-O-sulfotransferase accentuates neutrophil infiltration during acute inflammation in mice. Blood. 2012; 120(8):1742–51. [PubMed: 22791291]
55. Chen Q, Jin M, Yang F, Zhu J, Xiao Q, Zhang L. Matrix metalloproteinases: inflammatory regulators of cell behaviors in vascular formation and remodeling. Mediators Inflamm. 2013; 2013:928315. [PubMed: 23840100]
56. Kolarova H, Ambruzova B, Svihalkova Sindlerova L, Klinke A, Kubala L. Modulation of endothelial glycocalyx structure under inflammatory conditions. Mediators Inflamm. 2014; 2014:694312. [PubMed: 24803742]
57. van Golen RF, van Gulik TM, Heger M. Mechanistic overview of reactive species-induced degradation of the endothelial glycocalyx during hepatic ischemia/reperfusion injury. Free Radic Biol Med. 2012; 52(8):1382–402. [PubMed: 22326617]
58. Tarbell JM, Simon SI, Curry FR. Mechanosensing at the vascular interface. Annu Rev Biomed Eng. 2014; 16:505–32. [PubMed: 24905872]

59. Lopez-Quintero SV, Cancel LM, Pierides A, Antonetti D, Spray DC, Tarbell JM. High glucose attenuates shear-induced changes in endothelial hydraulic conductivity by degrading the glycocalyx. PLoS One. 2013; 8(11):e78954. [PubMed: 24260138]

60. Forbes JM, Yee LT, Thallas V, Lassila M, Candido R, Jandeleit-Dahm KA, et al. Advanced glycation end product interventions reduce diabetes-accelerated atherosclerosis. Diabetes. 2004; 53(7):1813–23. [PubMed: 15220206]

61. Danese C, Vestri AR, D'Alfonso V, Deriu G, Dispensa S, Baldini R, et al. Do hypertension and diabetes mellitus influence the site of atherosclerotic plaques? Clin Ter. 2006; 157(1):9–13. [PubMed: 16669546]

62. Padberg JS, Wiesinger A, di Marco GS, Reuter S, Grabner A, Kentrup D, et al. Damage of the endothelial glycocalyx in chronic kidney disease. Atherosclerosis. 2014; 234(2):335–43. [PubMed: 24727235]

63. Vlahu CA, Lemkes BA, Struijk DG, Koopman MG, Krediet RT, Vink H. Damage of the endothelial glycocalyx in dialysis patients. J Am Soc Nephrol. 2012; 23(11):1900–8. [PubMed: 23085635]

64. Wang H, Zhu HQ, Wang F, Zhou Q, Gui SY, Wang Y. MicroRNA-1 prevents high-fat diet-induced endothelial permeability in apoE knock-out mice. Mol Cell Biochem. 2013; 378(1-2):153–9. [PubMed: 23467882]

65. Pillarisetti S, Paka L, Obunike JC, Berglund L, Goldberg IJ. Subendothelial retention of lipoprotein (a). Evidence that reduced heparan sulfate promotes lipoprotein binding to subendothelial matrix. J Clin Invest. 1997; 100(4):867–74. [PubMed: 9259586]

66. Oorni K, Pentikainen MO, Ala-Korpela M, Kovanen PT. Aggregation, fusion, and vesicle formation of modified low density lipoprotein particles: molecular mechanisms and effects on matrix interactions. J Lipid Res. 2000; 41(11):1703–14. [PubMed: 11060340]

67. Tedgui A, Lever MJ. The interaction of convection and diffusion in the transport of 131I-albumin within the media of the rabbit thoracic aorta. Circ Res. 1985; 57(6):856–63. [PubMed: 4064259]

68. Topper JN, Cai J, Falb D, Gimbrone MA Jr. Identification of vascular endothelial genes differentially responsive to fluid mechanical stimuli: cyclooxygenase-2, manganese superoxide dismutase, and endothelial cell nitric oxide synthase are selectively up-regulated by steady laminar shear stress. Proc Natl Acad Sci U S A. 1996; 93(19):10417–22. [PubMed: 8816815]

Highlights

- Apoptosis is elevated systemically in the high fat fed $ApoE^{-/-}$ mouse model
- GCX thickness and coverage are decreased in atheroprone region only (BCA)
- Local and systemic inflammation together lead to LDL retention and plaque formation

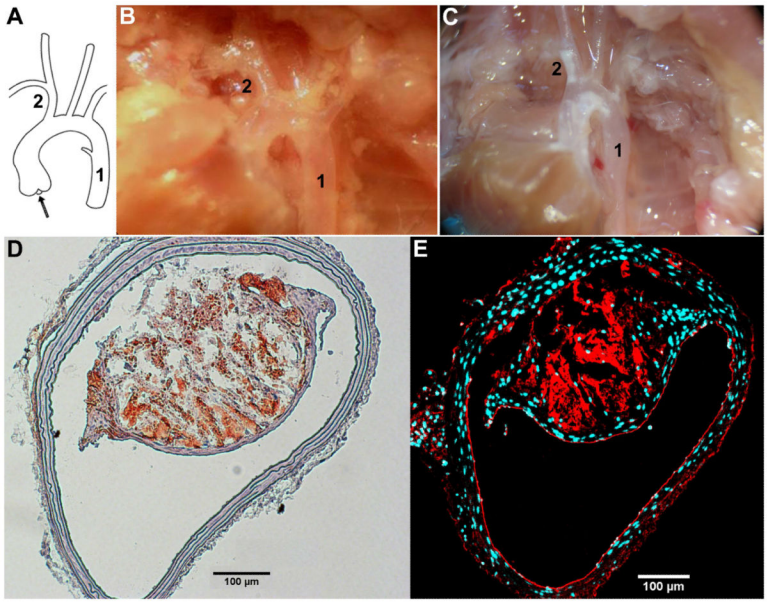

Fig. 1. Dissection of vessels from normal diet fed wild type mouse and high fat fed *ApoE*$^{-/-}$ mouse

(A) Schematic showing flow direction (arrow) of blood, 1% BSA, or 2% paraformaldehyde from the heart/aortic root and through the proximal branches of the vascular tree. (B) Picture of dissected wild type mouse on a normal diet, with clear vessels. (C) Picture of dissected *ApoE*$^{-/-}$ mouse on a high fat diet, with plaque filled (white streaks) vessels. The dissected vessels of interest are denoted by numbers 1 and 2, where 1 is the descending aorta (DA) and 2 is the brachiocephalic artery (BCA). (D) Representative image of Oil Red O stained lipid-laden plaque from the BCA of a high fat diet fed *ApoE*$^{-/-}$ mouse. (E) BCA of the same mouse immunostained for PECAM (red) demonstrates that, although a large plaque is present, endothelial cell coverage on the inner vessel wall can be seen on both the non-plaque and plaque regions. The staining also shows increased intra-plaque neo-vascularization. DAPI (blue) labels cell nuclei.

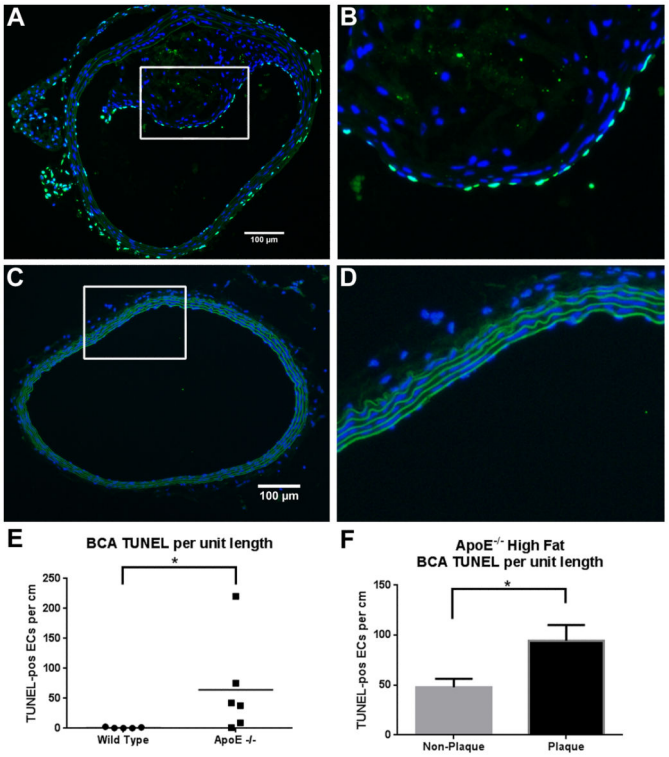

Fig. 2. Apoptosis in the BCA

Cross-sections shown in images A-D were stained for apoptosis using TUNEL. Cell nuclei are stained with DAPI (blue), elastin sheets auto-fluoresce in green, and apoptotic cells are labeled with FITC-TUNEL (bright green). (A) 20X image of the BCA obtained from a high fat fed *ApoE*$^{-/-}$ mouse, and (B) zoomed image of the boxed area in (A) showing elevated apoptosis. (C) 20X image of the BCA obtained from a normal diet fed wildtype mouse, and (D) zoomed image of the boxed area in (C) showing no sign of apoptosis. (E) TUNEL-positive ECs per cm in the in the wildtype *vs.* *ApoE*$^{-/-}$ (including plaque and non-plaque areas). N=86 sections from 6 animals for *ApoE*$^{-/-}$, N=73 sections from 5 animals for wild type (data points represent the mean of each animal); *p<0.0001 by non-parametric Mann-Whitney test. (F) TUNEL-positive ECs per cm in plaque and non-plaque areas of the *ApoE*$^{-/-}$ BCA. N=86 sections; *p<0.0001 by paired t-test.

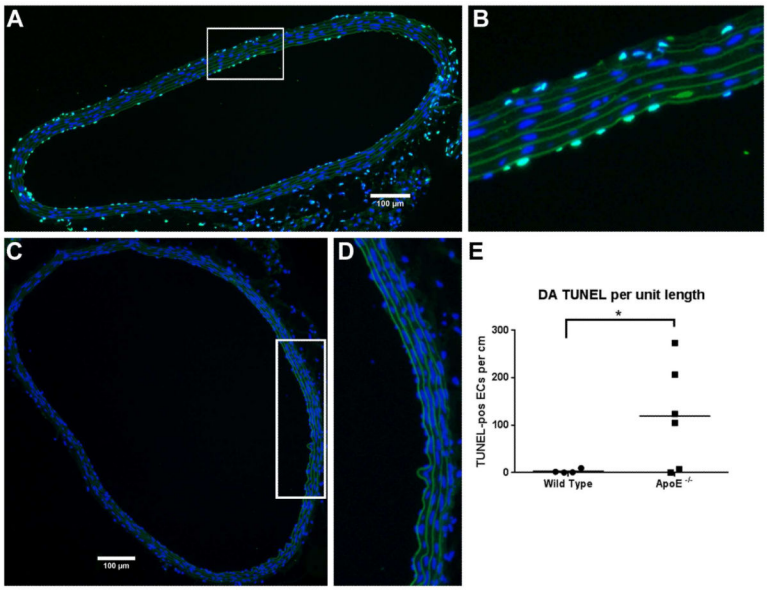

Fig. 3. Apoptosis in DA

Cross-sections shown in images A-D were stained for apoptosis using TUNEL. Cell nuclei are stained with DAPI (blue), elastin sheets auto-fluoresce in green, and apoptotic cells are labeled with FITC-TUNEL (bright green). (A) 20X image of the DA obtained from a high fat fed *ApoE*$^{-/-}$ mouse, and (B) zoomed image of the boxed area in (A) showing elevated apoptosis. (C) 20X image of the DA obtained from a normal diet fed wild type mouse, and (D) zoomed image of the boxed area in (C) showing no sign of apoptosis. (E) TUNEL-positive ECs per cm in the wild type *vs.* *ApoE*$^{-/-}$. N=97 sections from 6 animals for *ApoE*$^{-/-}$, N=67 sections from 4 animals for wild type (data points represent the mean of each animal); *p<0.0001 by non-parametric Mann-Whitney test.

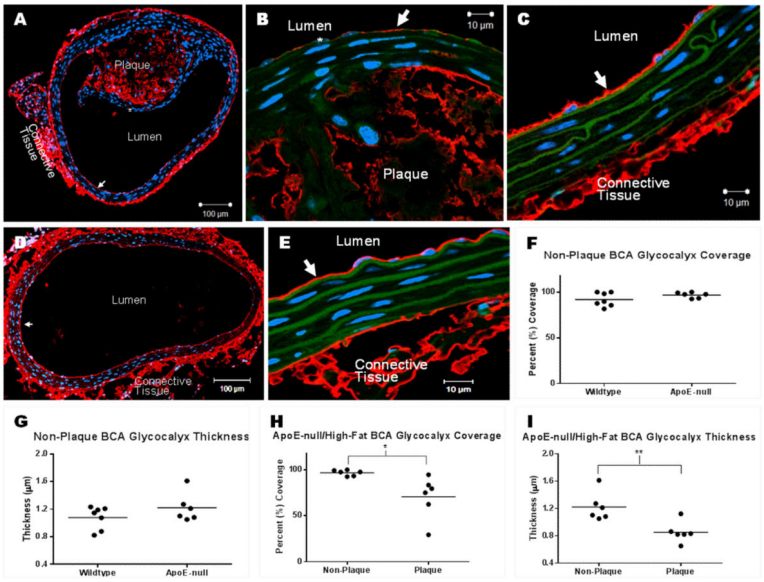

Fig. 4. GCX coverage and thickness in BCA sections stained with HABP to label the HA GCX component

(A) 10X image of a BCA with plaque, obtained from a high fat fed *ApoE*$^{-/-}$ mouse. GCX can be seen overlying non-plaque tissue (arrow) and is degraded overlying the plaque (star). (B) 63X/oil image of degraded GCX over plaque. Star indicates location of degraded GCX; arrow points to remaining GCX. (C) 63X/oil image of intact GCX (arrow) over the non-plaque region of diseased vessel. (D) 10X image of a healthy BCA without plaque and with fully intact GCX (arrow), obtained from a normal diet fed wildtype mouse. (E) 63X/oil image of intact GCX (arrow) in healthy vessel. (F-I) GCX quantification taken from 6-7 mice per condition. Mean comparisons were performed using unpaired t-tests. *$p < 0.05$; **$p < 0.01$.

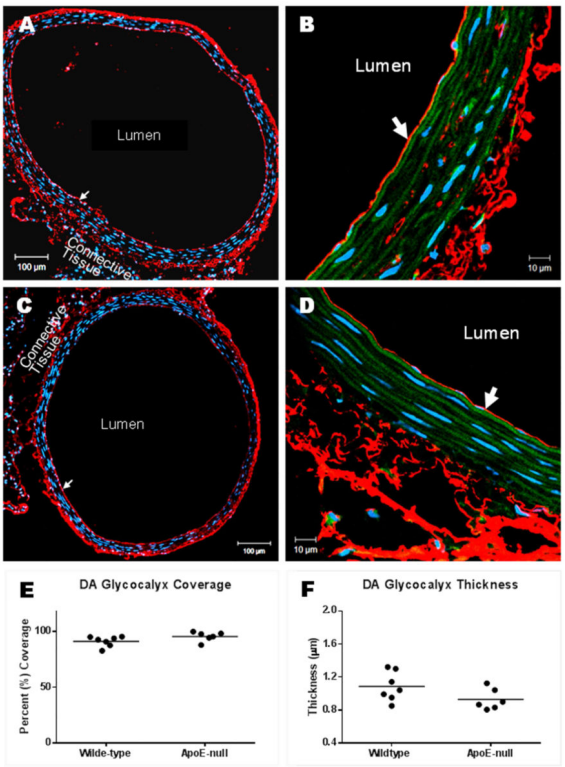

Fig. 5. GCX coverage and thickness in DA sections stained with HABP to label the HA GCX component

(A) 10X image of a DA obtained from a high fat fed *ApoE*$^{-/-}$ mouse. The GCX coats the entire inner vessel wall (arrow). (B) 63X/oil image of intact GCX shown in A; arrow points to the GCX. (C) 10X image of GCX (arrow) on DA obtained from a normal diet fed wildtype mouse. (D) 63X/oil image of intact GCX (arrow) shown in C. (E, F) GCX quantification taken from 6-7 mice per condition. Mean comparisons were performed using unpaired t-tests.

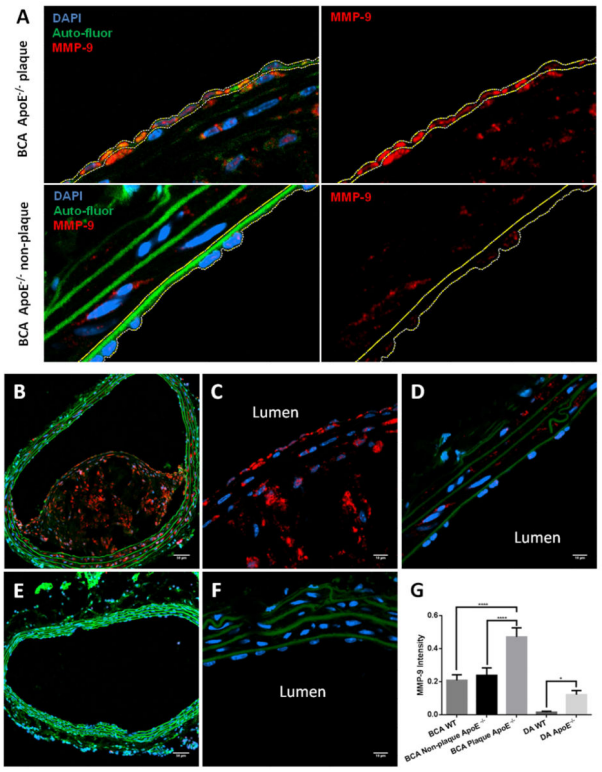

Fig. 6. MMP-9 staining in BCA sections

(A) Selection of the region of interest (ROI) for MMP-9 quantification in the endothelial layer. ROI was traced (yellow line) in the merged image (left panels) and quantified in the red channel (MMP-9; right panels). Typical selection areas are shown for the plaque (top panels) and non-plaque (bottom panels) areas of the *ApoE*$^{-/-}$ BCA. (B) 20X image of BCA with plaque, obtained from a high fat fed *ApoE*$^{-/-}$ mouse. MMP-9 staining (red) is seen throughout the plaque. (C) 63X/oil image of MMP-9 stain in the plaque. (D) 63X/oil image of MMP-9 stain in the non-plaque region of diseased vessel. (E) 20X image of a healthy BCA without plaque, obtained from a normal diet fed wildtype mouse, shows little MMP-9 staining. (F) 63X/oil image of MMP-9 stain in healthy vessel. (G) Quantification of MMP-9 intensity within the ROI as shown in (A). Mean comparisons were performed using 1-way ANOVA with Tukey's method to correct for multiple comparisons. N=33 for BCA samples; N=71 for DA WT; N=54 for DA *ApoE*$^{-/-}$. ****p<0.0001, *p<0.05. Scale bar = 50 μm for B and E; scale bar = 10 μm for C-D, F.

Table 1

Mean blood cholesterol concentration in wild type mice fed a normal chow diet and *ApoE*$^{-/-}$ mice fed a western diet. Numbers in parenthesis represent the percent of total cholesterol. $p<0.0002$ *vs.* wild type, for all types of cholesterol. n=4 for wild type; n=6 for *ApoE*$^{-/-}$

	Total cholesterol (mg/dL)	HDL (mg/dL)	LDL (mg/dL)	VLDL/Tri/CH (mg/dL)
Wild type	65.1 ± 1.8	31.5 ± 4.6	25.1 ± 2.5	8.4 ± 7.8
Normal diet		(48%)	(39%)	(13%)
ApoE $^{-/-}$	811.6 ± 53.6	6.5 ± 0.7	412.6 ± 14.6	392.6 ± 40.9
Western diet		(1%)	(51%)	(48%)